

Forearc structure beneath southwestern British Columbia: A three-dimensional tomographic velocity model

K. Ramachandran,¹ S. E. Dosso, and G. D. Spence

School of Earth and Ocean Sciences, University of Victoria, Victoria, British Columbia, Canada

R. D. Hyndman

Pacific Geoscience Centre, Geological Survey of Canada, Sidney, British Columbia, Canada

School of Earth and Ocean Sciences, University of Victoria, Victoria, British Columbia, Canada

T. M. Brocher

U.S. Geological Survey, Menlo Park, California, USA

Received 24 June 2004; revised 26 November 2004; accepted 8 December 2004; published 24 February 2005.

[1] This paper presents a three-dimensional compressional wave velocity model of the forearc crust and upper mantle and the subducting Juan de Fuca plate beneath southwestern British Columbia and the adjoining straits of Georgia and Juan de Fuca. The velocity model was constructed through joint tomographic inversion of 50,000 first-arrival times from earthquakes and active seismic sources. Wrangellia rocks of the accreted Paleozoic and Mesozoic island arc assemblage underlying southern Vancouver Island in the Cascadia forearc are imaged at some locations with higher than average lower crustal velocities of 6.5–7.2 km/s, similar to observations at other island arc terranes. The mafic Eocene Crescent terrane, thrust landward beneath southern Vancouver Island, exhibits crustal velocities in the range of 6.0–6.7 km/s and is inferred to extend to a depth of more than 20 km. The Cenozoic Olympic Subduction Complex, an accretionary prism thrust beneath the Crescent terrane in the Olympic Peninsula, is imaged as a low-velocity wedge to depths of at least 20 km. Three zones with velocities of 7.0–7.5 km/s, inferred to be mafic and/or ultramafic units, lie above the subducting Juan de Fuca plate at depths of 25–35 km. The forearc upper mantle wedge beneath southeastern Vancouver Island and the Strait of Georgia exhibits low velocities of 7.2–7.5 km/s, inferred to correspond to ~20% serpentinization of mantle peridotites, and consistent with similar observations in other warm subduction zones. Estimated dip of the Juan de Fuca plate beneath southern Vancouver Island is ~11°, 16°, and 27° at depths of 30, 40, and 50 km, respectively.

Citation: Ramachandran, K., S. E. Dosso, G. D. Spence, R. D. Hyndman, and T. M. Brocher (2005), Forearc structure beneath southwestern British Columbia: A three-dimensional tomographic velocity model, *J. Geophys. Res.*, *110*, B02303, doi:10.1029/2004JB003258.

1. Introduction

[2] As part of ongoing studies to better characterize the Cascadia subduction boundary, this article reports a three-dimensional (3-D) high-resolution compressional wave velocity model for the forearc of the northern Cascadia subduction zone. The velocity model was constructed through tomographic inversion of earthquake arrivals recorded by the permanent seismograph network in southern Vancouver Island and northwestern Washington

state as well as arrivals generated by a marine air gun array and recorded by a temporary seismograph array during the 1998 Seismic Hazards Investigation in Puget Sound (SHIPS) experiment [Fisher *et al.*, 1999; Brocher *et al.*, 1999, 2001].

[3] The crustal structure beneath Vancouver Island and adjoining regions, and the geometry of the subducting Juan de Fuca plate have been investigated by a large number of regional seismic reflection, seismic refraction, gravity, magnetic, and teleseismic receiver function studies [e.g., Riddihough, 1979; McMechan and Spence, 1983; Spence *et al.*, 1985; Clowes *et al.*, 1987; Hyndman, 1988; Hyndman *et al.*, 1990; Kurtz *et al.*, 1990; Dehler and Clowes, 1992; Cassidy and Ellis, 1991, 1993; Cassidy, 1995; Clowes *et al.*, 1997; Zelt *et al.*, 2001]. These studies defined landward

¹Now at Pacific Geoscience Centre, Geological Survey of Canada, Sidney, British Columbia, Canada.

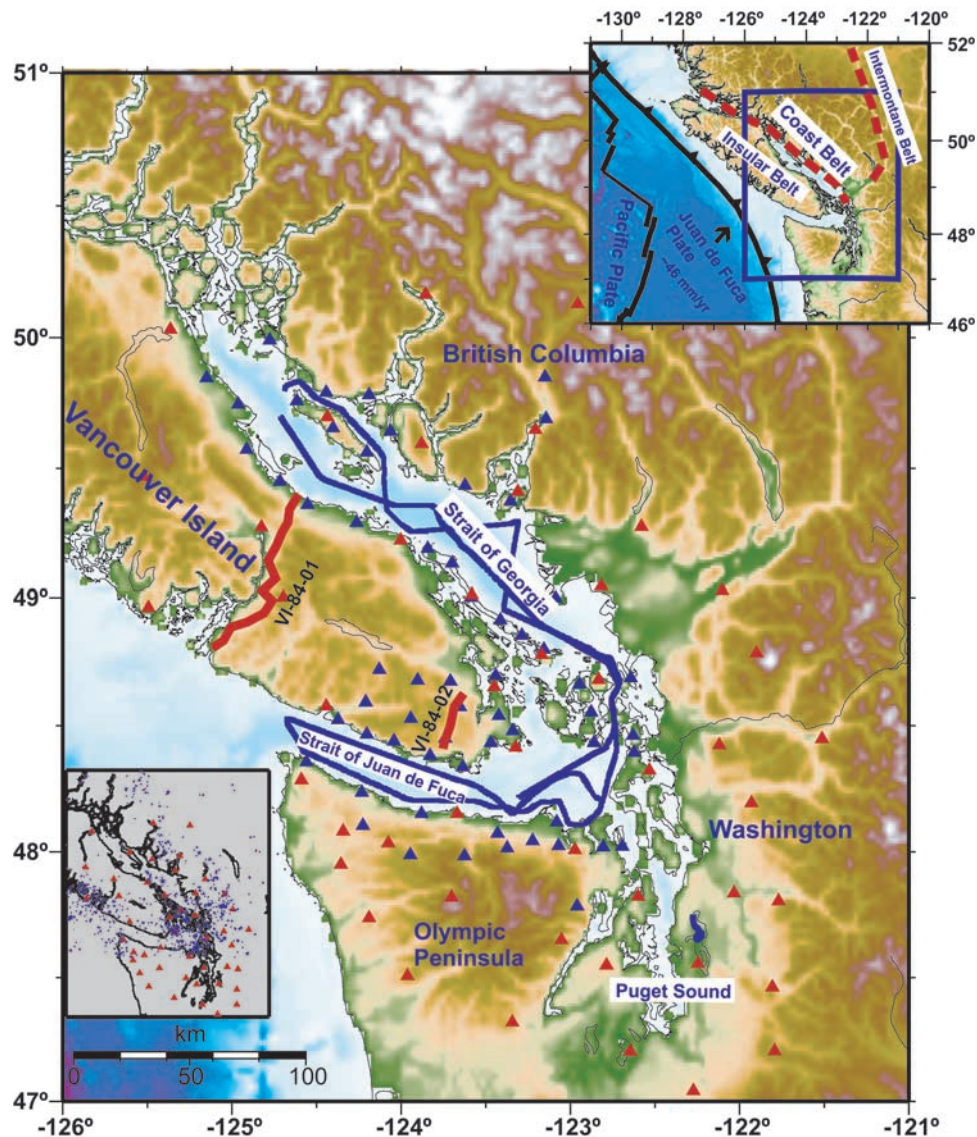


Figure 1. Location map showing the earthquake recording stations (red triangles) and SHIPS receivers (blue triangles) and shots (blue lines) used in the present study. Top inset shows the plate tectonic regime, and bottom inset shows the distribution of the earthquakes (blue stars) used in this study. Locations of two onshore seismic reflection lines VI-84-01 and VI-84-02 from Vancouver Island [Clowes *et al.*, 1987] are shown by the red lines.

dipping boundaries of terranes accreted from the Mesozoic through the Cenozoic.

[4] In this study, a new 3-D P wave velocity model for southwestern British Columbia and northern Washington state is constructed through joint inversion of 16,000 first-arrival times from approximately 1450 earthquakes recorded at 46 permanent recording stations, and 35,000 first-arrival times from the 1998 SHIPS experiment recorded at 58 temporary recording stations (Figure 1). The P wave velocity model provides the first detailed velocity structure of the forearc crust and upper mantle, and of the subducting Juan de Fuca plate beneath southern Vancouver Island and adjoining waterways.

[5] The subsurface velocity structure of the Wrangellia terrane and the volcanic Crescent terrane are inferred from the velocity model. Higher than average velocities are

imaged at some locations in the mid to lower Wrangellian crust composed of Palaeozoic to Mesozoic volcanic arc assemblage, similar to the velocities imaged by *Fliedner and Klemperer* [1999] in the eastern Aleutian island arc terrane. Low forearc mantle velocities of 7.2–7.5 km/s imaged in the forearc mantle are similar to the velocities reported for subduction zones in central Japan [*Kamiya and Kobayashi*, 2000], eastern Aleutians [*Fliedner and Klemperer*, 1999], Andes [*Myers et al.*, 1998; *Graeber and Asch*, 1999], and northern Costa Rica [*DeShon and Schwartz*, 2004].

2. Geology, Tectonics, and Seismicity

[6] About 200 My ago the Intermontane superterrane, made up mostly of sedimentary and volcanic rocks,

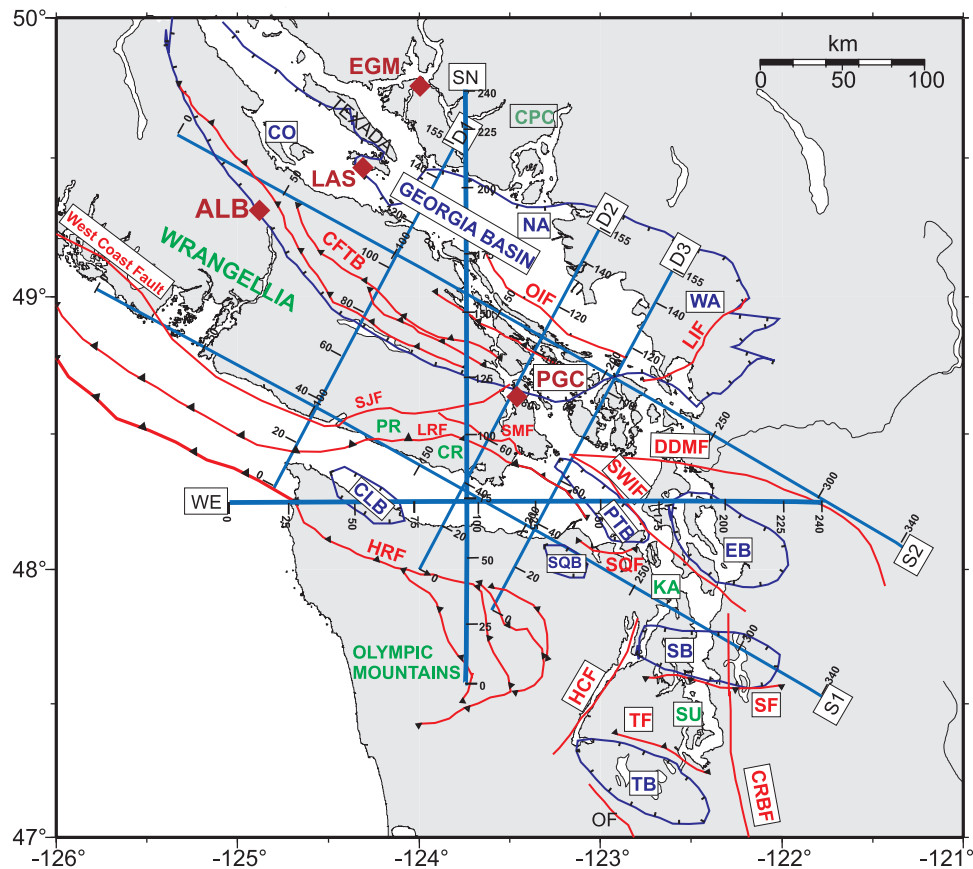


Figure 2. Map showing sedimentary basins and faults. Major geologic features taken from *Muller [1977]*, *England and Bustin [1998]*, *Brocher et al. [2001]*, and *Van Wagoner et al. [2002]*. CFTB, Cowichan Fold and Thrust Belt; CH, Chuckanut subbasin; CLB, Clallam basin; CO, Comox subbasin; CPC, Coast Plutonic Complex; CRBF, Coast Range boundary fault; CR, Crescent terrane; DDMF, Darrington-Devils Mountain fault; EB, Everett basin; HCF, Hood Canal fault; HRF, Hurricane Ridge fault; LIF, Lummi Island fault; LRF, Leech River fault; NA, Nanaimo subbasin; OF, Olympia fault; OIF, Outer Islands fault; PR, Pacific Rim terrane; PTB, Port Townsend basin; SB, Seattle basin; SF, Seattle fault; SJF, San Juan fault; SMF, Survey Mountain fault; SQB, Sequim basin; SQF, Sequima fault; SU, Seattle uplift; SWIF, Southern Whidbey Island fault; TB, Tacoma basin; TF, Tacoma fault; WA, Whatcom subbasin. ALB, LAS, EGM, and PGC are permanent recording stations. D1, D2, D3, S1, S2, SN, and WE show the location of the vertical cross sections shown in Figures 7, 8, and 9.

collided with the North America plate (Figure 1, top inset). Around mid-Cretaceous time, the last major collisional episode emplaced the Insular superterrane against the Intermontane superterrane, and generated the mid-Cretaceous to early Tertiary intrusive rocks of the Coast Belt in the suture region [Monger et al., 1982; Monger, 1990] (Figure 1, top inset). The two superterranes underlie the Intermontane and Insular belts, respectively (Figure 1, top inset). Vancouver Island is dominated by Wrangellia terrane, emplaced during the middle Cretaceous [Smith and Tipper, 1986], composed of Devonian through Lower Jurassic igneous sequences and sedimentary successions (Figure 2) and is thought to represent a largely Jurassic island arc [Jones et al., 1977; Muller, 1977]. The Coast Belt lies to the east of Wrangellia and straddles the mid-Cretaceous suture zone between the Insular and Intermontane superterranes.

[7] The Pacific Rim and Crescent terranes were the last to accrete to the continent and reached their present locations during late Cretaceous and Tertiary periods [Johnson,

1984]. The mainly Mesozoic metasedimentary Pacific Rim terrane and the Eocene volcanic Crescent terrane lie along the west coast and southern end of Vancouver Island, respectively (Figure 2). In southern Vancouver Island, the Pacific Rim terrane is separated from Wrangellia by the San Juan and Survey Mountain fault systems (Figure 2). Mafic rocks of the Crescent terrane composed of basalt, diabase and gabbro, are considered correlative to the Metchosin volcanics of southern Vancouver Island [Muller, 1980]. Massey [1986] proposed that the Metchosin volcanics formed as new oceanic crust in a marginal basin. To the south of Vancouver Island, the Strait of Juan de Fuca lies in the synclinal depression formed by the Crescent terrane. To the east of Vancouver Island, the Strait of Georgia is a forearc basin that straddles the boundary of the Insular and Coast belts.

[8] The Juan de Fuca oceanic plate converges with the North America continental plate at a relative rate of ~ 46 mm/a directed N56°E [Riddihough and Hyndman, 1991]. The Olympic Subduction Complex to the south of

Vancouver Island is an exposed former accretionary wedge, metamorphosed and uplifted as a result of subduction [e.g., *Brandon and Calderwood*, 1998]. To the east of the Olympic Subduction Complex, the Puget Lowland is a modern forearc basin continuous with the Georgia basin to the north (Figure 2). The Crescent terrane along the eastern margin of the Olympic Subduction Complex is tilted to the east by the uplift of the Olympic Subduction Complex rocks [e.g., *Brandon and Calderwood*, 1990].

[9] Subduction of the Juan de Fuca plate beneath the North America plate along the northern Cascadia margin has resulted in a number of damaging earthquakes [e.g., *Rogers*, 1998]. The shallower earthquakes occur in the overriding North American continental crust and the deeper Wadati-Benioff earthquakes occur within the subducting Juan de Fuca plate. Both crustal and deeper Wadati-Benioff events are concentrated in the northern Cascadia margin. In southwestern British Columbia, a few correlations of faulting with seismicity have been reported, e.g., the 1946 $M = 7.3$ event with the Beaufort Range and associated faults in central Vancouver Island [*Rogers and Hasegawa*, 1978], and the 1997 $M = 4.6$ event with an active fault imaged by seismic reflection data in the northern Strait of Georgia [*Mosher et al.*, 2000; *Cassidy et al.*, 2000].

3. Tomographic Inversion

[10] In this paper, seismic tomography of active source and earthquake travel times is used to construct a 3-D velocity model of the subsurface. In such inversions, the number of parameters in the model space exceeds the number of data points, such that regularization of the inversion is needed. *Toomey et al.* [1994] utilized horizontal and vertical smoothing as regularization constraints and termed this approach an “adaptive inverse modeling tool.” *Zelt and Barton* [1998] regularized inversion by penalizing total model roughness and employing a “jumping” strategy [*Shaw and Orcutt*, 1985].

[11] The tomographic algorithm employed in the present study applies a regularized inversion scheme similar to that of *Benz et al.* [1997]. The method was implemented by generalizing the regularized inversion described by *Zelt and Barton* [1998] and the corresponding “first-arrival seismic tomography” code to simultaneously invert earthquake and active source data for 3-D P wave velocity model and relocated hypocentral parameters (location and origin time). Joint inversion of active source and earthquake data provides additional constraints on the shallow velocity structure which in turn provides improved constraints on the earthquake hypocentral parameters. A summary of the methodology for joint inversion of earthquake and active source data is provided here; details are given by *Ramachandran* [2001].

[12] The body wave travel time T_{ij} from an earthquake i to a seismic station j can be expressed as

$$T_{ij} = t_{ij} - \tau_i, \quad (1)$$

where t_{ij} is the absolute travel time and τ_i is the earthquake origin time. Given the travel time t_{ij}^{obs} measured at station i of a network of I permanent recording stations for the j th earthquake, the travel time t_{ij}^{cal} is calculated using the initial hypocentral location and origin time and an initial slowness model. The misfit between the observed and calculated

travel time is the residual Δt_{ij} . For J earthquakes, the total number of parameters to be determined in the inversion are $L + 4J$, where L represents the number of velocity model parameters. For a finite parametrization of the slowness model the linearized equation can be written as

$$\Delta t_{ij} = \sum_{l=1}^L \frac{\partial T_{ij}}{\partial m_l} \Delta m_l + \sum_{k=1}^3 \frac{\partial T_{ij}}{\partial x_{jk}} \Delta x_{jk} + \Delta \tau_j, \quad (2)$$

where m_l represent the L parameters of the slowness model; $\partial T_{ij}/\partial m_l$ represent the partial derivatives of the slowness model parameters ($l = 1, L$), and $\partial T_{ij}/\partial x_{jk}$ are the partial derivatives of the hypocenter location parameters for the earthquakes ($j = 1, J$). The slowness and hypocenter parameter updates are represented by Δm_l and Δx_{jk} , respectively, and the computed earthquake origin time updates are given by $\Delta \tau_j$.

3.1. Method

[13] This tomographic inversion method is based on iterative linearized inversion of the travel time equations, regularized by minimizing the vertical and horizontal roughness of the model subject to fitting the travel time data to within estimated uncertainties using the χ^2 criterion. The objective function Φ minimized at each iteration is

$$\Phi(\mathbf{m}) = \Delta \mathbf{t}^T \mathbf{C}_d^{-1} \Delta \mathbf{t} + \lambda [\mathbf{m}^T \mathbf{C}_h^{-1} \mathbf{m} + s_z \mathbf{m}^T \mathbf{C}_v^{-1} \mathbf{m}], \quad (3)$$

where \mathbf{m} is the slowness model vector; $\Delta \mathbf{t}$ is the travel time data residual vector; \mathbf{C}_d is a diagonal matrix representing the variance of the travel time measurements; \mathbf{C}_h and \mathbf{C}_v are the horizontal and vertical roughening matrices, respectively; λ is the trade-off parameter; and s_z sets the relative importance of maintaining horizontal to vertical model smoothness. Three-dimensional anisotropic Laplacian smoothing was implemented by 2-D and 1-D finite difference smoothers in the horizontal and vertical directions, respectively. Uncertainty estimates for hypocentral parameters were not used to regularize the hypocentral position. Rather, the travel time data constrain the hypocentral positions. The noise present in the data is assumed to be Gaussian, in which case the acceptable data misfit is set to the expected value for the normalized χ^2 misfit statistic, i.e., $\Delta \mathbf{t}^T \mathbf{C}_d^{-1} \Delta \mathbf{t} / (N - 1) = 1$, where N is the number of data. Equation (3) is solved by the method described by *Zelt and Barton* [1998].

[14] The two free parameters to be decided are λ and s_z . The parameter s_z that sets the horizontal to vertical model smoothness is initially tested for a range of values and is subsequently held fixed throughout the inversion. λ is the trade-off parameter between data misfit and model smoothness. For large values of λ , model smoothness is emphasized over fitting the data. As the value of λ decreases, the relative importance of fitting the data increases. During the inverse procedure, the parameter λ is tested over a range of values by slowly decreasing it from a starting value. The starting value of λ and the reduction factor are chosen such that small steps are taken in the model space in order for the linearization assumption to be honored.

3.2. Data

[15] The 1998 SHIPS active source experiment recorded arrivals from a total of 33,000 air gun shots fired on 11 shot

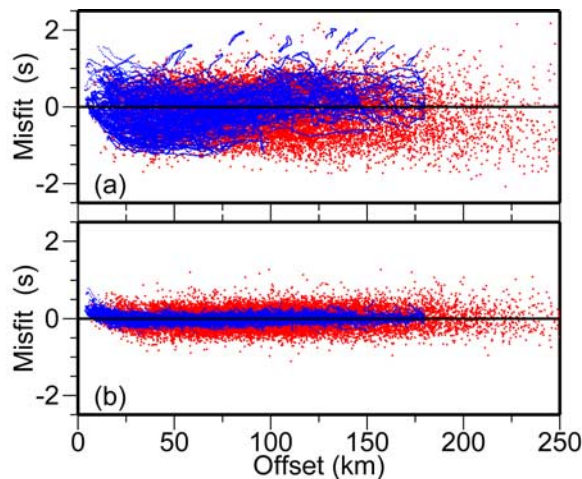


Figure 3. (a) Travel time misfit for initial 1-D velocity model and (b) travel time misfit for final 3-D velocity model. Red dots correspond to the earthquake events, and blue dots correspond to the SHIPS active source events.

lines in the waterways of the Strait of Georgia, the Strait of Juan de Fuca, and Puget Sound (Figure 1) [Brocher *et al.*, 1999]. Approximately 35,000 SHIPS first-arrival travel time picks recorded at 58 temporary land based stations, extracted from the 175,000 picks employed by Ramachandran *et al.* [2004] in a high-resolution upper crustal tomography study, were included in the joint inversion. The travel times were picked manually and the quality was assessed on the basis of shot receiver distance. Picking errors were estimated based on shot receiver distance and were used to assign observational uncertainties for the travel time picks. Variable pick uncertainty values of 50, 70, and 90 ms were assigned to picks having first-arrival travel times less than 10 s, 10–15 s, and greater than 15 s, respectively. These unreduced travel times correspond to source receiver offsets less than 65 km, 65–100 km, and greater than 100 km, respectively.

[16] First arrival travel times from approximately 1450 earthquakes recorded at 46 permanent recording stations between 1983 and 2000 (Figure 1, bottom inset) were extracted from the earthquake catalog of the Pacific Geoscience Centre, Geological Survey of Canada. Earthquake selection criteria included earthquakes from all depth levels, above magnitude 1.0, and recorded by at least six stations within the study region. These criteria resulted in approximately 16,000 picks from 1450 earthquakes, with depths that ranged from 1 to 90 km. The initial hypocenter locations and origin times obtained from the earthquake catalog were used as the starting hypocentral parameters for the tomographic inversion. The earthquake travel time observations were assigned an uncertainty of 100 ms.

3.3. Inversion

[17] The velocity model was parameterized in both forward and inverse steps by a node and cell spacing of $(3 \times 3 \times 3)$ km. The velocity model dimensions in (x, y, z) directions are $(360 \times 450 \times 93)$ km. The top of the model was set to 3 km above sea level to allow positioning the receivers at their actual elevations in the velocity model. An

initial 1-D velocity model was constructed that best fit the time-distance plot and was consistent with the regional geology. Computation of travel times in a velocity model is the forward step of the inverse problem. Vidale's method [Vidale, 1990] calculates first-arrival travel times on a uniform grid by solving the Eikonal equation using the finite difference method. Travel time grids are computed for the velocity model using Vidale's computation scheme modified by Hole and Zelt [1995] for handling large velocity contrasts and implemented in the first-arrival seismic tomography code [Zelt and Barton, 1998]. The travel time at a particular receiver location is obtained by linear interpolation of the travel times at eight surrounding grid nodes. For active source data, ray path length is computed by tracing the gradient direction from receiver to source position. For earthquake data, the ray is traced along the gradient direction from the earthquake position to the recording station. Rays were traced in the travel time grid after each iteration to account for the change in the hypocenter parameters between iterations. During the tomographic inversion, perturbation updates for the velocity and hypocentral parameters were computed simultaneously at each iteration, and the velocity model and hypocentral parameters were updated at each iteration.

[18] The travel time misfit for the initial model as a function of offset is shown in Figure 3a. The RMS travel time residual for this model for approximately 50,000 picks was 479 ms for a normalized χ^2 of 42. The inversion was then run in test mode with a series of vertical to horizontal smoothing parameters ranging from 0.10 to 0.25. After inspecting the resulting models for vertical and horizontal roughness, the vertical to horizontal smoothing parameter was set to 0.2 (i.e., three times more smoothing in the horizontal direction than vertical direction) and was held

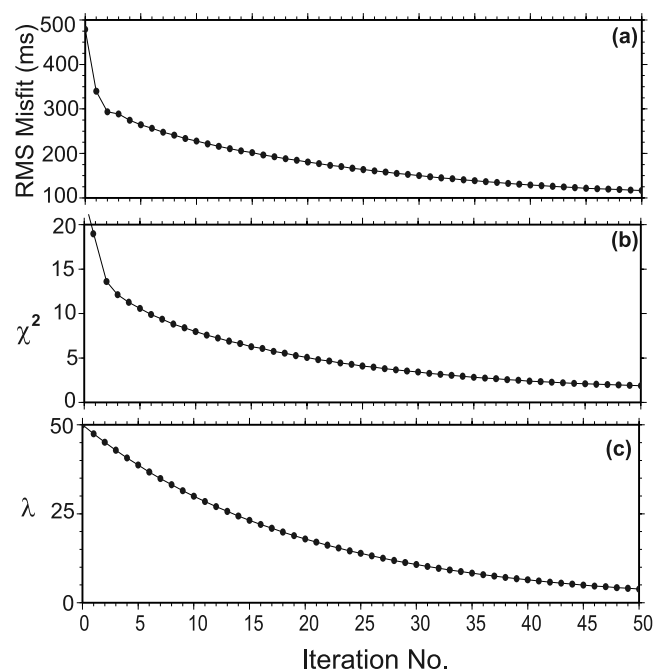


Figure 4. Convergence plot showing the reduction of (a) RMS misfit, (b) normalized χ^2 , and (c) the trade-off parameter λ , during inversion.

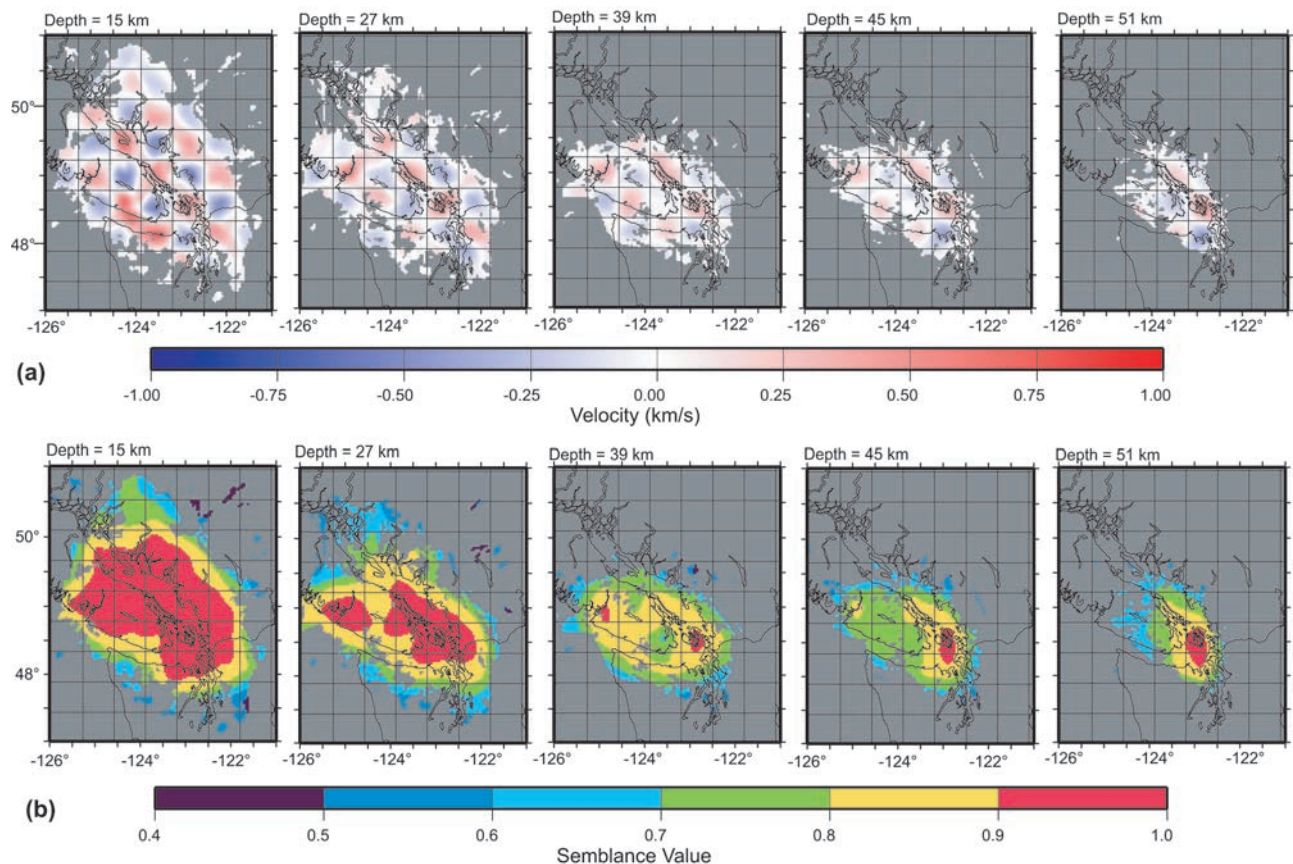


Figure 5. Depth slices of (a) checkerboard test recovered anomaly pattern and (b) semblance values for 50 km grid size at 15, 27, 39, 45, and 51 km depth.

fixed throughout the inversion. This value is close to the value of 0.25 used in the upper crustal tomographic study for this region [Ramachandran *et al.*, 2004]. After 46 iterations, a stable minima at an RMS misfit of ~ 120 ms and normalized χ^2 of ~ 2 was reached (Figure 4) and this model was selected as further iterations resulted in no further improvement to the solution. The travel time misfit with offset for the final model is uniform over the entire range of offsets for the SHIPS data and the earthquake events (Figure 3b). The bias at offset distances less than 15 km is possibly due to the difficulty in fitting the lateral and vertical velocity variation at shallow depths by a 3 km model parametrization. The earthquake relocations during the inversion averaged 0.8, 2.8, and 0.9 km in the E-W, N-S, and vertical directions, respectively. The maximum hypocenter change observed was less than 4.5 km from their starting (catalogue) values in the E-W, N-S, and vertical directions.

3.4. Checkerboard Tests

[19] Checkerboard tests with grid sizes of 30, 40 and 50 km were carried out to assess the ability of the data to resolve model features of these sizes at different depth levels. Semblance values [e.g., Zelt and Barton, 1998] between the input and output checkerboard anomaly patterns were computed with a window size of $33 \times 33 \times 6$ km. Semblance values of 1 and 0.5 indicate total recovery of the perturbation and no recovery of the pertur-

bation, respectively. For 30 and 40 km grid sizes, computed semblance values suggest adequate lateral resolution down to 21 and 33 km depth, respectively [Ramachandran, 2001]. The Recovered checkerboard anomaly pattern for the 50 km grid size (Figure 5a) indicates that the ray coverage is sufficient to recover features of the order of 50 km lateral extent over the entire depth of the model. Semblance plot for the 50 km grid size (Figure 5b) suggests the presence of reliable lateral resolution in the center of the model and poor resolution over the edges of the model at all depths. The lower semblance on the edges of the model is caused by decreased range of directivity in the ray coverage within the cells. The recovered anomaly pattern and semblance values for a vertical checkerboard test for a grid size 10 km, extracted along vertical cross section S1 (Figure 6; location of the cross section in Figure 2), a vertical resolution of ~ 10 km is inferred at depths below 25 km. In the upper crust, the recovered vertical checkerboard anomaly pattern and semblance values show that the velocity structure is well constrained and vertical resolution in the upper crust is 5–10 km.

[20] It is inferred from the horizontal and vertical checkerboard test results (Figures 5a and 6a), and semblance values (Figures 5b and 6b) that the roughness observed in the vertical cross sections (Figures 7, 8, and 9; location of the cross sections in Figure 2) at upper crustal levels is reliable. Vertical model roughness is expected based on the geometry and structure of the accreted terranes beneath

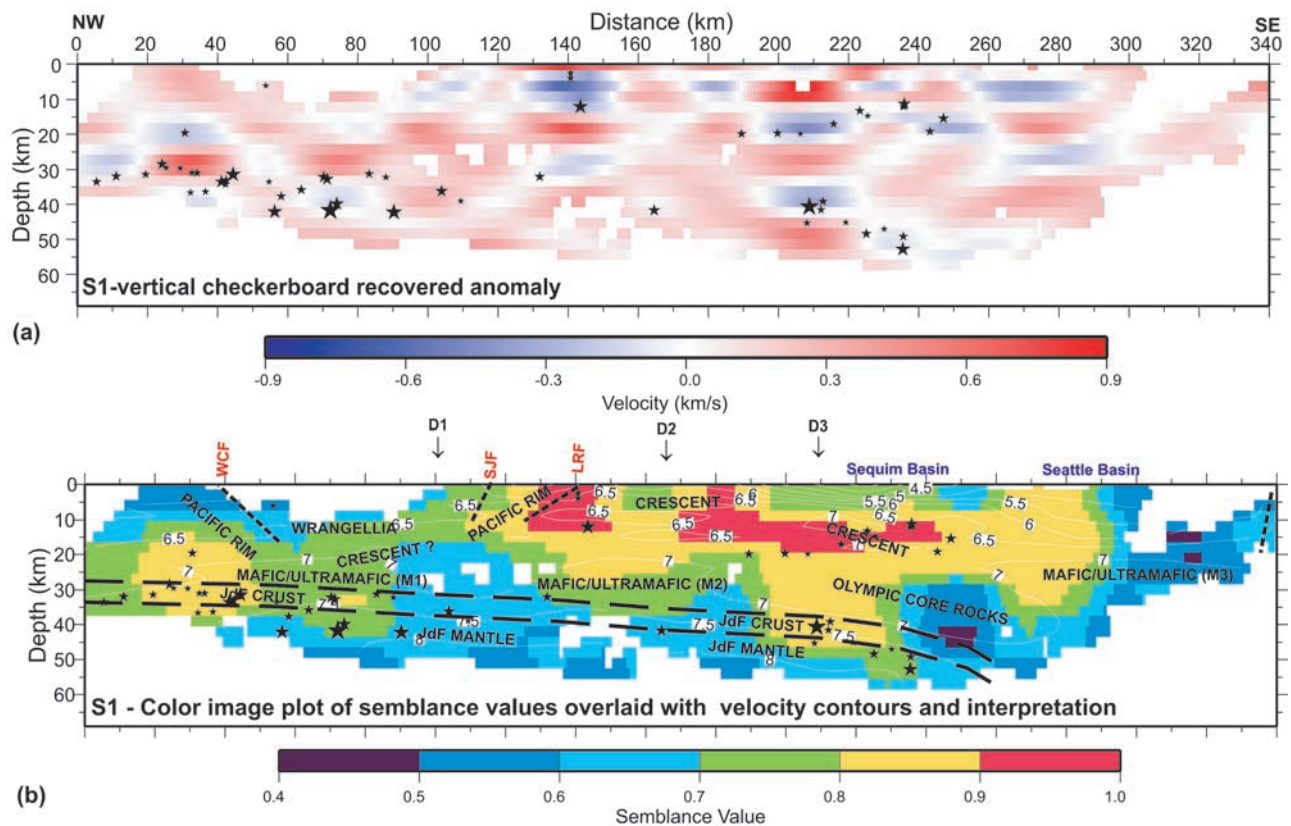


Figure 6. (a) Vertical checkerboard test (10 km vertical grid) recovered anomaly pattern along vertical cross section S1 (location of cross section in Figure 2). (b) Semblance values plotted as color image. P wave velocity contours and interpretation from Figure 8a are superposed.

Vancouver Island inferred from reflection seismic studies by *Clowes et al.* [1987] and *Hyndman et al.* [1990]. The model roughness in the upper crustal structure is constrained well by the large-scale, high-quality, SHIPS active source data. Well constrained upper crustal velocity structure enhances better relocation of earthquakes in the upper crust and also increases the resolution of deeper structure by constraining the segment of the rays that travel through the upper crust from beneath. The velocity model is parameterized on a 3 km cell spacing in this study. To accommodate the velocity variations in the upper crust, the cell boundaries will have a small amount of roughness across the boundaries. Much smoother velocity model can be constructed if the model is parameterized with a finer cell spacing. However, with a finer cell spacing the number of rays passing through a given cell would decrease resulting in poor solution quality in the inversion procedure.

4. Interpretation of the 3-D Velocity Model

[21] The final P wave velocity model is shown as vertical cross sections along selected orientations (Figures 7, 8, and 9; location of the cross sections in Figure 2), as horizontal velocity slices (Figure 10), and as isovelocity plot of 6.0 km/s (Figure 11a). Relocated earthquake locations plotted on the vertical cross sections are projected from within 5 km horizontal on either side of the cross sections. The geometry and velocity structure of the

forearc crust and upper mantle, and the subducting Juan de Fuca crust and upper mantle beneath Vancouver Island and adjoining regions are inferred from the velocity model.

4.1. Forearc Crust

[22] The forearc crust in the study region is composed mainly of the accreted terranes lying beneath southern Vancouver Island and the Straits of Juan de Fuca and Georgia, and of the Olympic Subduction Complex in northwestern Washington.

4.1.1. Wrangellia

[23] The Wrangellia terrane, a Palaeozoic to Mesozoic volcanic arc assemblage, accreted to western North America in the mid Cretaceous, underlies much of southern Vancouver Island and the Strait of Georgia [e.g., *Yorath and Nasmith*, 1995]. Upper crustal velocities range from 6.0 to 6.5 km/s between model distance 80–140 km on cross section D1 (Figure 7a). A similar crustal velocity structure is observed on the northeastern end of the cross sections D2 and D3 (Figures 7a and 7b), and at the western margin of the Strait of Georgia in the depth slices at 12, 18, and 24 km (Figure 10). It is inferred from the isovelocity surface map (Figure 11a) that the velocities of Wrangellia rocks exceed 6.0 km/s at depths of ~ 3 km. The velocity model associates the Wrangellian lower crust with slightly higher than average crustal velocities (Figure 7) at some locations. Lower crustal velocities of the Wrangellia rocks on cross sections D1, D2, D3, and S2, range from 6.5 to 7.2 km/s (Figures 7 and 8b). These velocities are in general higher

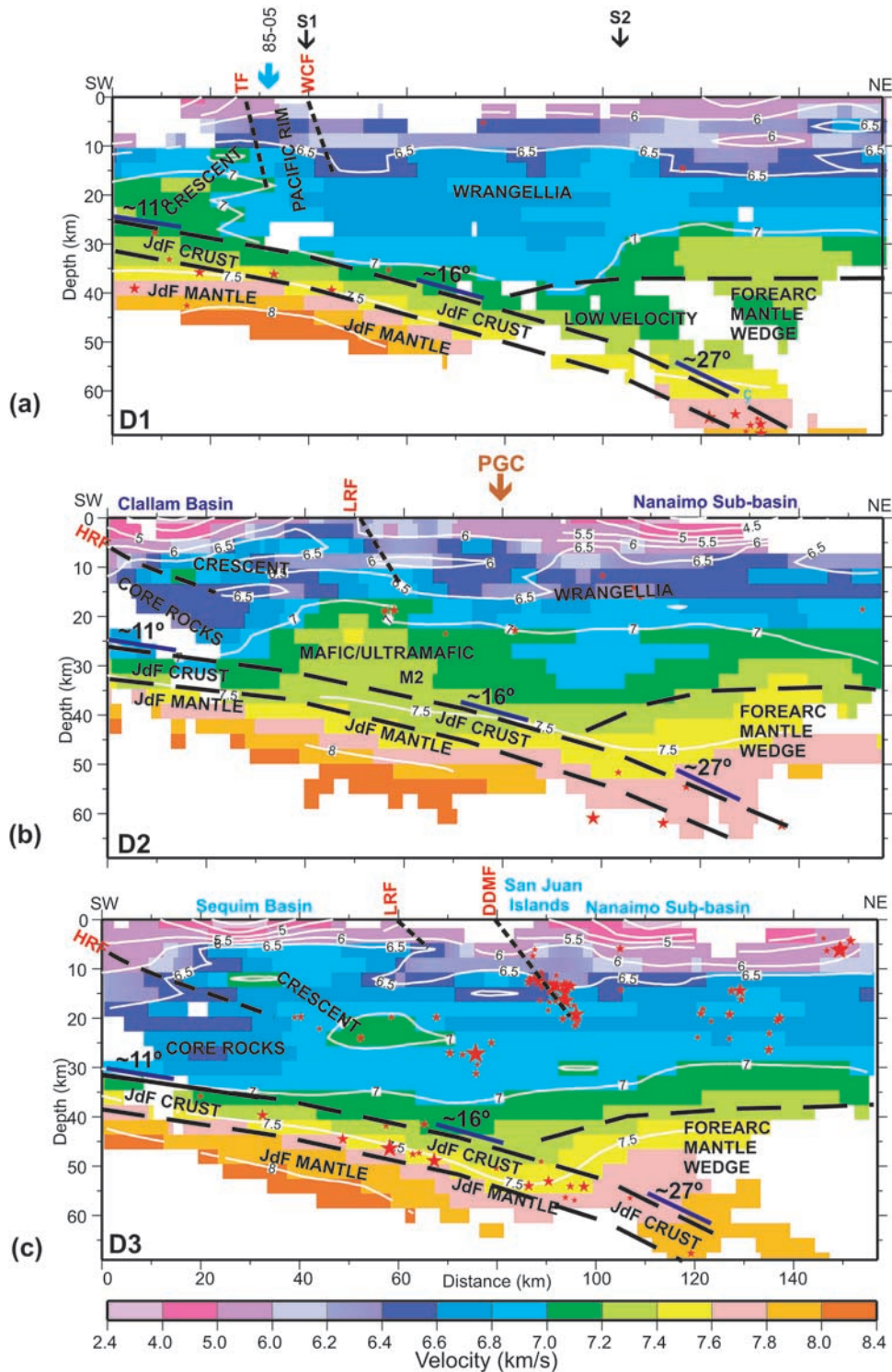


Figure 7. Vertical velocity sections (a) D1, (b) D2, and (c) D3, along the dip direction of Juan de Fuca plate subduction. TF, Tofino Fault; WCF, Westcoast Fault; other abbreviations are as in Figure 2.

than the velocities observed in average continental crust [Christensen and Mooney, 1995].

[24] The higher than average crustal velocities (6.5 to 7.2 km/s) imaged in the mid to lower crust of the Wrangellia terrane are typical for island and continental volcanic arcs [Mooney and Meissner, 1991; Miller and Christensen, 1994; Flidner and Klempner, 1999]. In a laboratory study,

Miller and Christensen [1994] measured P wave velocities of rock samples from a 40 km thick exposed section of the Kohistan-Ladakh terrane in northern Pakistan, recognized as a remnant Mesozoic intraoceanic island arc. The velocities from our tomographic velocity model are similar to their laboratory measured velocities of 6.2 km/s at 2–13 km depth and 6.7–7.0 km/s at 13–30 km depth. The

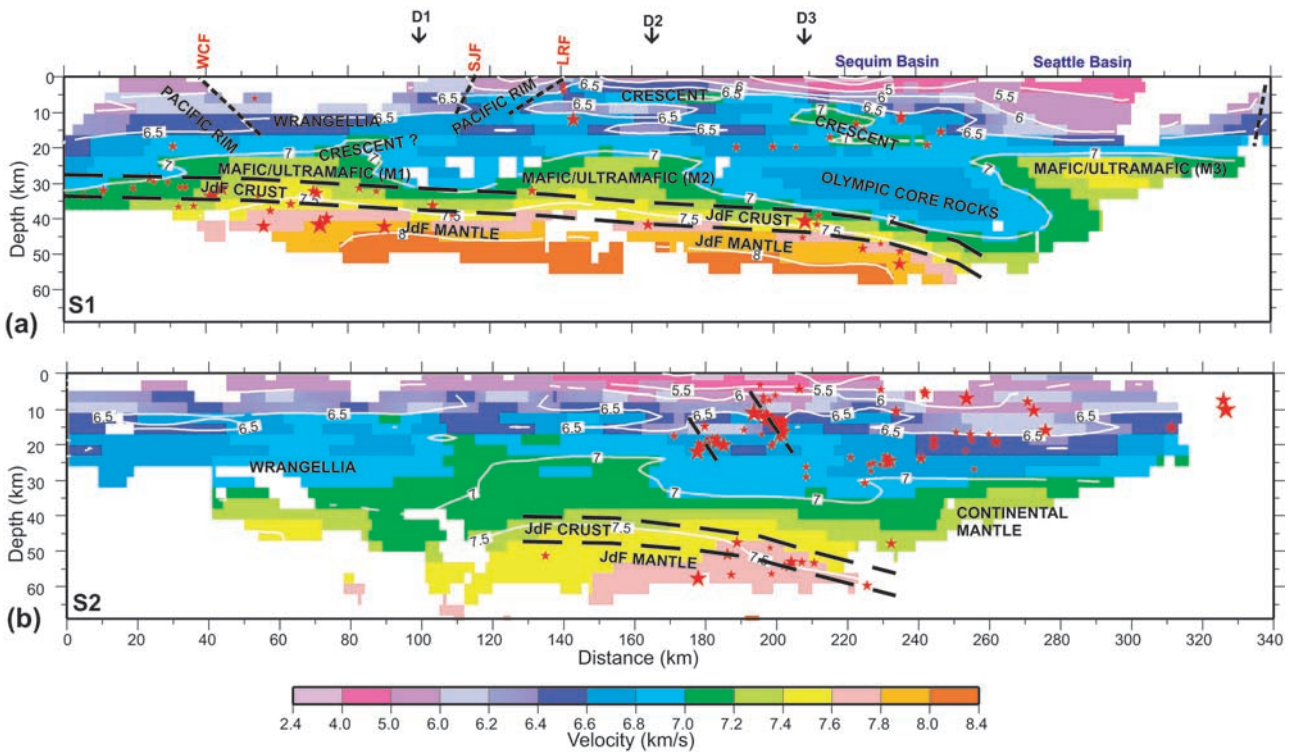


Figure 8. Vertical velocity sections (a) S1 and (b) S2 along the strike direction of Juan de Fuca plate subduction. M1, M2, and M3 represent the inferred mafic and/or ultramafic units. WCF, Westcoast Fault; other abbreviations are as in Figure 2.

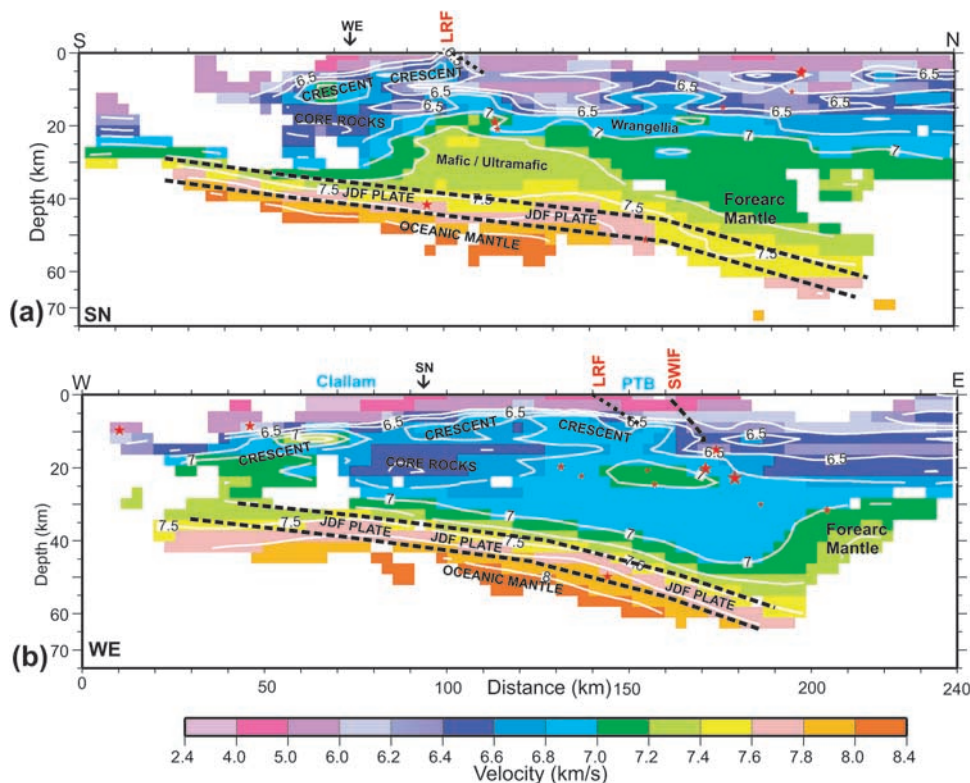


Figure 9. Vertical velocity sections (a) SN and (b) WE showing the inferred location of core rocks beneath Crescent terrane. Abbreviations are as in Figure 2.

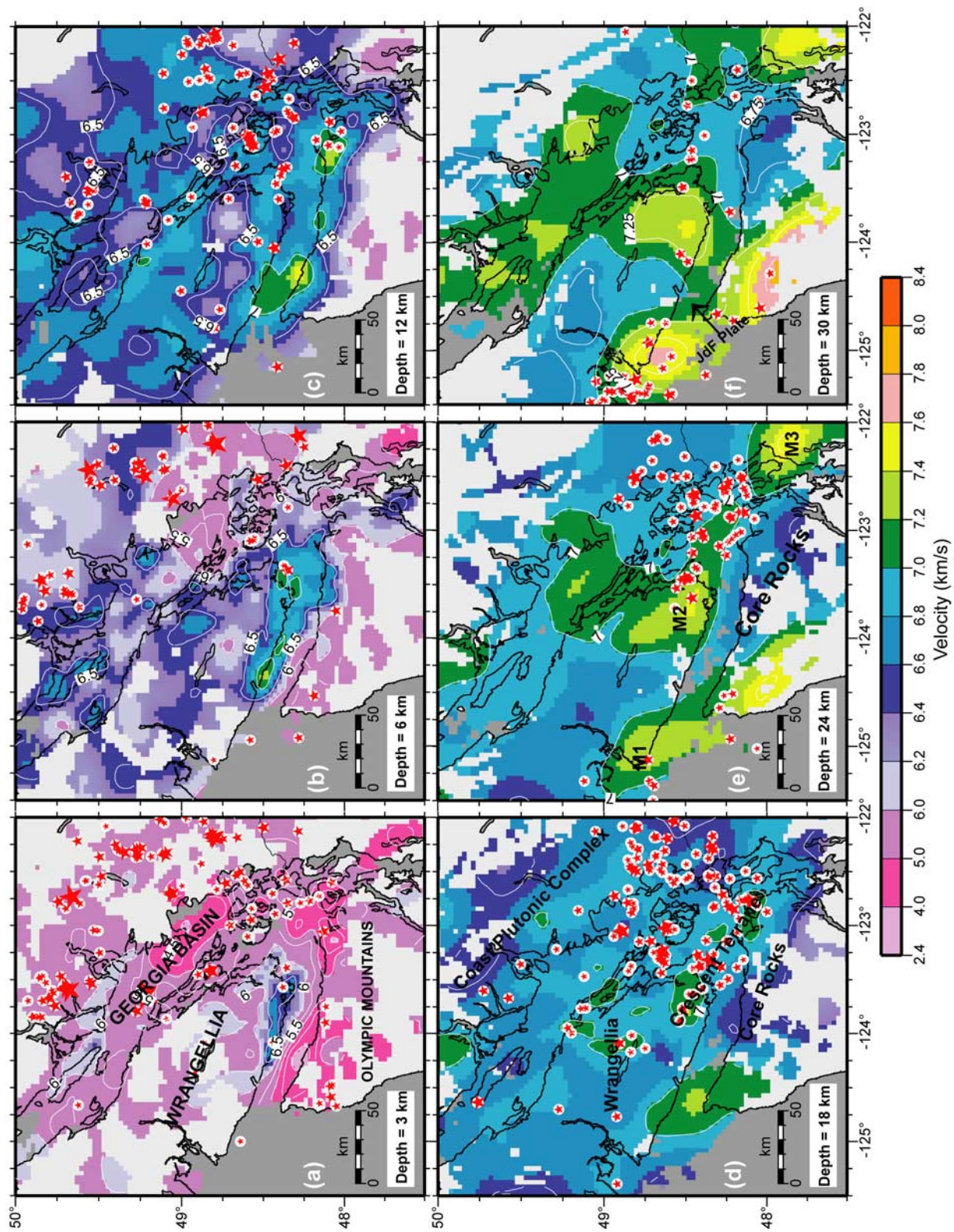


Figure 10. Horizontal velocity sections at (a) 3 km, (b) 6 km, (c) 12 km, (d) 18 km, (e) 24 km, and (f) 30 km depths. M1, M2, and M3 in Figure 10e represent the three inferred mafic/ultramafic units. Abbreviations are as in Figure 2.

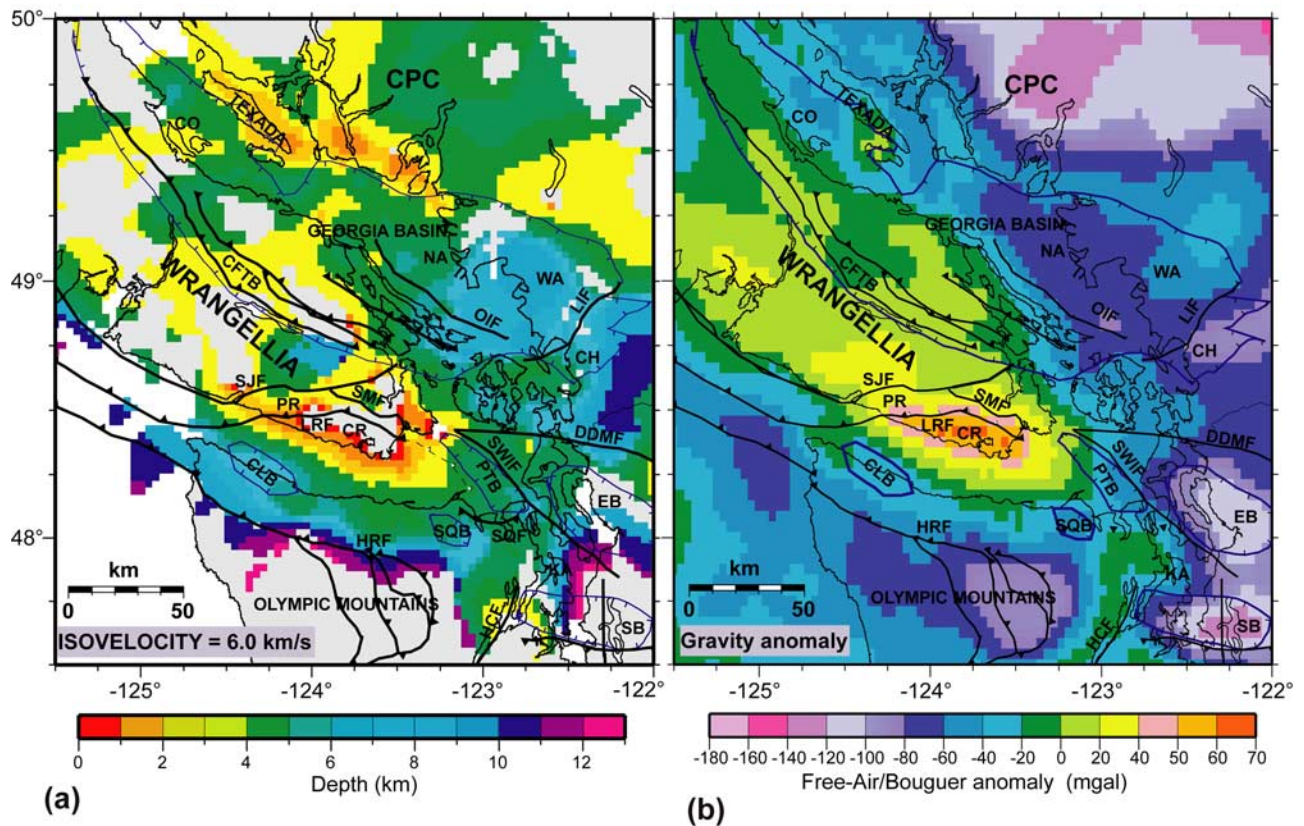


Figure 11. (a) Isovelocity surface map at 6.0 km/s. (b) Gravity anomaly map (data from the National Geophysical Data Center, USA CD-ROM). Abbreviations as in Figure 2.

computed crustal P wave velocity for the Cascades, Wrangellia, and the Kohistan accreted terrane average at 6.70 ± 0.05 km/s [Miller and Christensen, 1994]. Fliedner and Klemperer [1999] discussed the similarity of the velocity structure of the eastern Aleutian island arc to that of the exposed accreted island arc terranes of Talkeetna in southern Alaska and Kohistan in northern Pakistan. They computed an average crustal velocity of 6.7 km/s, similar to the values computed for the Kohistan accreted terrane by Miller and Christensen [1994]. The higher than average velocities observed in the mid to lower Wrangellian crust in our study are inferred to be due to the presence of mafic and possibly ultramafic rocks.

4.1.2. Crescent Terrane

[25] The Eocene volcanic Crescent terrane underlies the northern Strait of Juan de Fuca at shallow depth and is exposed on the southern tip of Vancouver Island and the northern Olympic Peninsula (Figures 10a and 10b). The shallow depth to the top of Crescent terrane and its areal extent beneath southern Vancouver Island and the Strait of Juan de Fuca is inferred from the 6.0 km/s isovelocity plot (Figure 11a). This feature correlates well with a prominent gravity high on southern Vancouver Island (Figure 11b). In the Strait of Juan de Fuca, the top of Crescent terrane deepens southward (Figures 10b and 11a) and the Crescent terrane rocks underlying the eastern end of Clallam basin (location on Figure 2) are identified from the higher than average upper crustal velocities (~ 6.5 km/s) that extend to a depth of ~ 20 km (Figures 7b, 10c, and 10d). The Olympic Subduction Complex rocks with velocities less

than 6.5 km/s are inferred to be thrust beneath the Crescent terrane at model distance 0–20 km (Figure 7b).

[26] The thickness of the Crescent Terrane rocks was estimated to be less than 10 km beneath southern Vancouver Island from reflection studies [Clowes *et al.*, 1987; Hyndman *et al.*, 1990; Calvert, 1996] and gravity modeling [Dehler and Clowes, 1992; Clowes *et al.*, 1997]. Graindorge *et al.* [2003] employed SHIPS wide-angle data and gravity data from southern Vancouver Island and interpreted the extension of the Crescent terrane beneath the Strait of Juan de Fuca below 10 km depth. At model distance 0–30 km on cross section D1 (Figure 7a), higher velocities imaged in the range of 6.5–7.2 km/s at depths of 10–20 km are inferred to represent the Crescent terrane rocks. The estimated depth to the top of the Juan de Fuca crust at this location from seismic reflection studies is 22–25 km [Hyndman *et al.*, 1990]. On cross section D1 (Figure 7a), between model distances 0 and 30 km the higher velocities imaged at depths of 10–25 km are inferred to represent the Crescent terrane rocks which extend down to the top of the subducting Juan de Fuca crust.

[27] Eocene Crescent terrane rocks, including the Metchosin Oceanic Igneous Complex in southern Vancouver Island [Muller, 1977; Massey, 1986], are considered correlative with the Siletz terrane along the Oregon-Washington margin [e.g., Clowes *et al.*, 1987; Tréhu *et al.*, 1994; Parsons *et al.*, 1998, 1999]. Outcrops of the Metchosin igneous complex in southern Vancouver Island are composed of volcanics, layered gabbro and sheeted dikes [e.g., Massey, 1986]. P wave velocities of gabbro range from 6.8

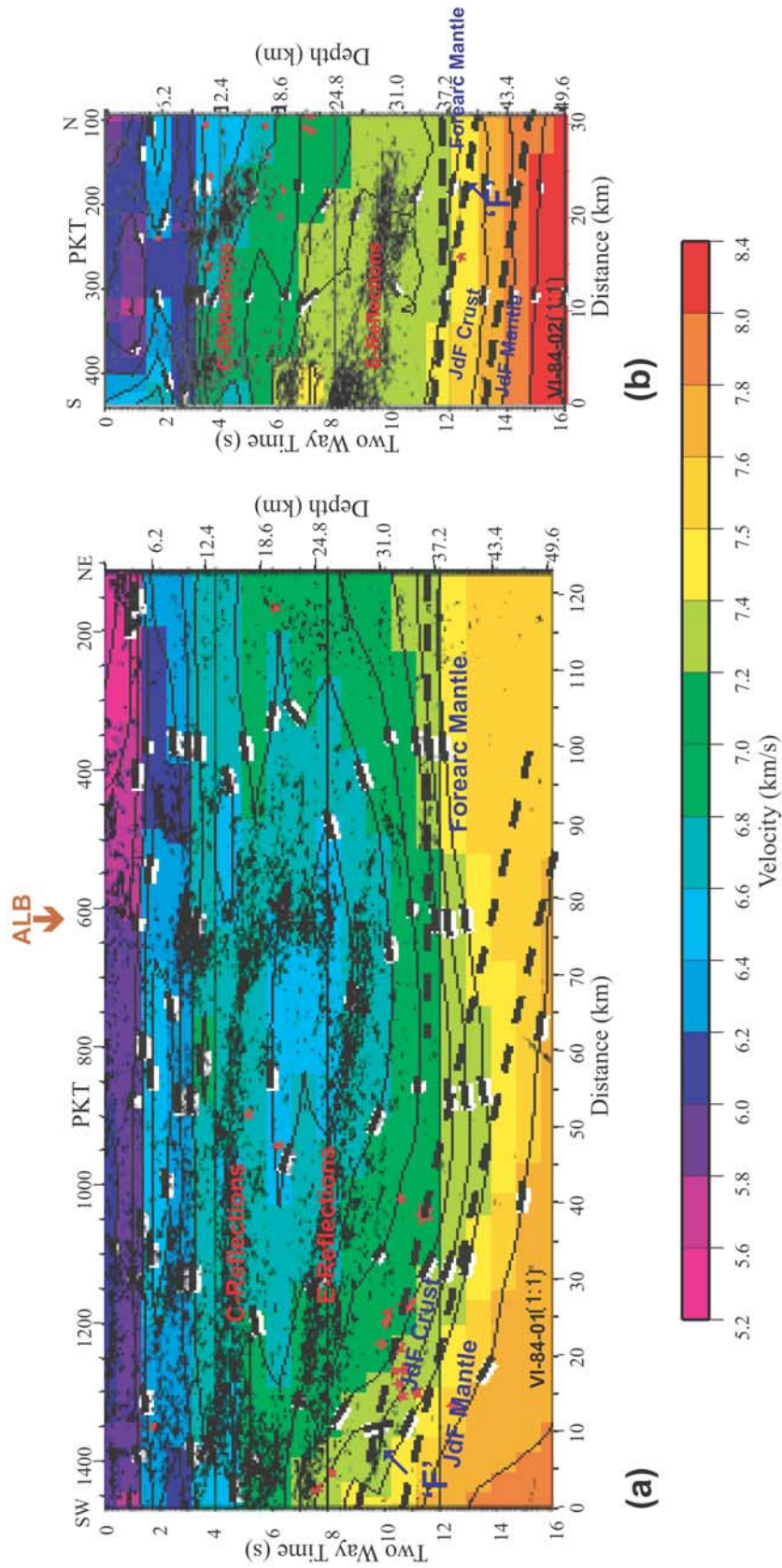


Figure 12. Tomographic velocity overlaid on seismic reflection lines (line locations in Figure 1) from southern Vancouver Island (a) line VI-84-01 and (b) line VI-84-02. ALB refers to the location of the permanent recording station projected on the seismic line.

to 7.2 km/s corresponding to a depth range of 5 to 35 km [Christensen and Mooney, 1995]. Laboratory measurements of the P wave velocities in the Crescent terrane volcanic rocks range from 5.5–6.9 km/s [Brocher and Christensen, 2001]. Velocities above ~ 7.0 km/s imaged in the upper crust in our model are too high for basaltic rocks at this depth. Gabbroic complexes are observed at Metchosin Igneous Complex in southern Vancouver Island and Blue Hills in Washington state. From a 3-D tomographic study, Van Wagoner *et al.* [2002] identified upper crustal velocities beneath the Puget Sound region in the range of 7–7.5 km/s and attributed these velocities to gabbro emplaced with in the Crescent terrane. We associate the higher velocities in the range of 6.8–7.2 km/s imaged beneath southern Vancouver Island to gabbro emplacement in the Crescent terrane, similar to the interpretations of Parsons *et al.* [1999] and Van Wagoner *et al.* [2002] in Puget Sound region.

4.1.3. Olympic Subduction Complex

[28] Eocene and younger clastic sedimentary rocks scraped off the incoming Juan de Fuca plate are accreted as a thick accretionary prism along the central Cascadia subduction zone margin to form the shelf and continental slope. Locally the prism has been metamorphosed, uplifted and exposed as the Olympic Subduction Complex in the Olympic peninsula [e.g., Brandon and Calderwood, 1990] (Figure 1). Laboratory measurements of the P wave velocities in the Core rocks of the Olympic Subduction Complex range from 5.0 to 6.25 km/s at confining pressures up to 1 Gpa (equivalent to a depth of ~ 30 km) [Brocher and Christensen, 2001]. In laboratory studies, the Crescent terrane volcanic rocks exhibit a velocity contrast of up to 1.0 km/s with the low-velocity Core rocks of the Olympic Subduction Complex that underthrust them in the Olympic peninsula [Brocher and Christensen, 2001].

[29] The northern limit of underthrusting of the Core rocks beneath Crescent terrane is inferred to lie just south of Vancouver Island where higher-velocity rocks (6.5 km/s and above) extend from near surface to 20 km depth (Figures 7a, 7b, 9a, and 9b). In cross section SN (Figure 9a), between model distances of 50 and 80 km and at depths of 15 to 25 km, low-velocity Core rocks are inferred to underthrust the Crescent terrane rocks and extend downward to the top of the subducting Juan de Fuca crust. A gravity anomaly low at this location (Figure 11b) correlates with the inferred presence of Core rocks of low-velocity and low-density material in the subsurface. On the WE cross section (Figure 9b), low velocities imaged beneath high velocity between model distances of 70 and 130 km are inferred to represent the Core rocks underthrusting the Crescent terrane. North of the Strait of Juan de Fuca, such underthrusting of low-velocity accreted rocks to depths greater than 30 km is not imaged on the cross sections D1, D2, D3, and S2 (Figures 7 and 8b).

4.1.4. Deep Mafic and/or Ultramafic Units

[30] Gravity and seismic reflection and refraction studies [e.g., White and Savage, 1965; Riddihough, 1979; Spence *et al.*, 1985; Clowes *et al.*, 1987] first identified high velocity, high-density crustal rocks beneath southern Vancouver Island. We identify three regions M1, M2, and M3 above the subducting slab in the range of 7.0–7.5 km/s that are likely lenses of mafic/ultramafic rocks (Figure 10e). These

three regions lie beneath Barkley Sound on the western margin of Vancouver Island, southern Vancouver Island, and central Puget Lowland (Figure 8a). At these locations the vertical checkerboard tests indicate adequate resolution for a vertical grid size of 10 km (Figure 6a). Semblance values greater than 0.7 are observed at the locations of the interpreted high-velocity units M1, M2, and M3 (Figure 6b), suggesting that structures of dimension 10 km and greater are reliably recovered.

[31] Unit M1 correlates with the high-velocity unit reported by Spence *et al.* [1985] and Drew and Clowes [1990], having a velocity of ~ 7.2 km/s at a depth of 20 km. The mafic and/or ultramafic unit M2, mapped beneath southern Vancouver Island, appears to be continuous with the high-velocity Crescent terrane which lies directly above it (Figures 9a and 10a). Unit M2 may represent either mafic gabbros in the Crescent terrane or a lens of ultramafic mantle still attached to the base of the Crescent terrane. M2 coincides with a high-velocity lens identified at station PGC (Figure 2) [Cassidy, 1995] at a depth of ~ 21 km. M2 also correlates with a similar higher-velocity unit (7.6 km/s) identified by Graindorge *et al.* [2003] beneath the Strait of Juan de Fuca. Unit M3 correlates with a zone of higher than average velocity (7.5–8.0 km/s) previously mapped between continental crust and the subducted slab beneath the central Puget lowland [Symons and Crosson, 1997; Stanley *et al.*, 1999; Van Wagoner *et al.*, 2002]. The high-velocity anomalies possibly represent the basal gabbro members of the underthrust Crescent terrane.

4.2. Juan de Fuca Plate

[32] Little velocity contrast is expected at the contact of the forearc lower crust with the underlying oceanic Juan de Fuca slab crust. The main velocity contrast associated with the Juan de Fuca plate is expected at the interface between the oceanic crust (6.75–7.0 km/s) and the oceanic mantle (8.0–8.2 km/s). In the smoothed velocity model constructed here, this interface is taken at an intermediate velocity of ~ 7.5 km/s and the top of the oceanic crust is approximately 7.0 km higher, assuming an average oceanic crustal thickness. A smoothed 7.5 km/s contour and the relocated earthquake hypocenters on the vertical cross sections are used to define the position of the top of the Juan de Fuca mantle. The top of the Juan de Fuca crust is drawn 7 km above the defined position of the top of the oceanic mantle. The downgoing plate is resolved in most of the sections. The Juan de Fuca plate dip estimated from the gradient of the interpreted interface between the forearc crust and the oceanic crust on the cross sections D1, D2, and D3 is $\sim 11^\circ$, 16° , and 27° at depths of 30, 40, and 50 km, respectively.

[33] The earthquakes observed in profile D1 between 60 and 70 km depth are inferred to lie in the subducting Juan de Fuca slab (Figure 7a), consistent with results from receiver function studies by Cassidy and Ellis [1993]. The estimated depth of ~ 42 km to the top of the Juan de Fuca crust beneath station PGC (Figure 7b) from this study is close to the estimate of ~ 45 km by Cassidy [1995]. In cross sections D3 (Figure 7c) and S1 (Figure 8a), the position of the Juan de Fuca plate is well defined by the velocity structure and the relocated hypocenters.

[34] The maximum age of the subducting Juan de Fuca plate at the deformation front is 9 Ma, and such a young

lithosphere is thin, flexible, and buoyant due to the high ratio of less dense crust to more dense mantle [e.g., Rogers, 1983]. Young lithosphere is negatively buoyant only after the basaltic rocks in the oceanic crust undergo a phase change to high-density eclogite. Thermal modeling for warm slabs like Juan de Fuca show that metamorphic reactions in the subducting oceanic crust can start at 40–50 km depth [Peacock *et al.*, 2002]. This phase change appears to produce a bend in the young lithosphere at ~50 km depth. The downward slab bending associated with such a phase change and the slab pull may result in Wadati-Benioff slab earthquakes [Rogers, 1983]. This is consistent with the hypothesis that the earthquakes that lie within the slab crust are probably induced by the dehydration-embrittlement processes in the slab crust [e.g., Kirby *et al.*, 1996]. Hacker *et al.* [2003] suggested that some of the deeper earthquakes in the Juan de Fuca slab could be due to deserpentinization reactions in the slab mantle. On vertical cross sections D1, D2, and D3 (Figure 7), the change in slope of the Juan de Fuca slab from ~16° at 40 km depth to ~27° at 50 km is probably due to slab densification during dehydration reactions in the slab.

4.3. Forearc Upper Mantle: Serpentinization

[35] The depth to the Cascadia forearc crust/mantle interface is approximately 36 km (Figure 7), assuming that velocities greater than 7.4 km/s correspond to the top of the forearc mantle in this region. Cassidy and Ellis [1993] estimated a similar depth to the forearc mantle at station LAS (location in Figure 2) through receiver function studies.

[36] The forearc upper mantle wedge corner exhibits velocities of 7.2–7.5 km/s (Figure 7). Low *P* wave velocities in the forearc mantle have been reported from other subduction zones. Kamiya and Kobayashi [2000] imaged low *P* wave velocities of 6.9 km/s in the forearc mantle beneath central Japan and DeShon and Schwartz [2004] determined forearc mantle wedge velocity of 7.6 km/s in northern Costa Rica. In the eastern Aleutians, Fliedner and Klempner [1999] determined low forearc mantle velocities of 7.4 km/s. Graeber and Asch [1999] showed that the Andean forearc mantle beneath northern Chile exhibited low *P* wave velocities. The cause for low velocities in forearc mantle rocks can be due to partial melt or hydration and serpentinization of the mantle peridotites. Low-velocity zones imaged in the crust and mantle wedge beneath volcanic arcs associated with high temperature were interpreted to be partial melt zones by Zhao [2001]. Kamiya and Kobayashi [2000] associated low velocities in the forearc mantle beneath central Japan to serpentinization of the forearc mantle because of cool forearc temperatures.

[37] Hyndman and Peacock [2003] presented geological and geophysical evidence for forearc mantle serpentinization by fluids expelled from the subducting slab. The velocity observed in the northern Cascadia forearc mantle is anomalously low compared to the *P_n* velocity of 8.15–8.25 km/s in stable continental areas for an estimated Moho temperature of 350–450°C [e.g., Hyndman and Peacock, 2003]. *P* wave velocity of dry forearc mantle composed of depleted ultra mafic rocks (e.g., harzburgite, lherzolite and dunite) are in the range of 8.0–8.2 km/s. Cascadia forearc is

relatively cool as a consequence of heat removed by the subduction of cool near surface oceanic rocks. Observed heat flow in this region is in agreement with the subduction thermal model and calculated uppermost forearc mantle temperature is in the range of 400–600°C [Hyndman and Wang, 1995]. At temperatures less than 700°C, a number of hydrous minerals such as serpentine, talc and brucite may be generated in the forearc mantle wedge due to hydration [Peacock and Hyndman, 1999].

[38] The forearc upper mantle velocity in this region varies between 7.4 and 7.8 km/s [McMechan and Spence, 1983; Spence *et al.*, 1985; Miller *et al.*, 1997; Stanley *et al.*, 1999; Brocher *et al.*, 2003]. Serpentinization of peridotites by ~15–20% is necessary to lower *P* wave velocities to 7.8–7.4 km/s [Christensen and Mooney, 1995]. Beneath the Strait of Georgia, Zhao *et al.* [2001] mapped low *P* wave velocities at depths of 45–60 km, with a negative perturbation of approximately 6% about the initial reference model, inferring 15–20% serpentinization in the forearc mantle. Along an east trending profile in southern Cascadia, Bostock *et al.* [2002] inferred 50–60% serpentinization at the mantle wedge corner for an *S* wave velocity perturbation of 10% about a lower crustal shear wave velocity of 3.6 km/s. The serpentinization levels at the mantle wedge corner in this region estimated from *P* wave velocities are lower than those estimated from *S* wave velocities.

5. Comparison of Velocity Data With Seismic Reflection Data

[39] The multichannel seismic reflection lines VI-84-01 and VI-84-02 from onshore Vancouver Island [Clowes *et al.*, 1987] are overlaid on the tomographic velocity model (Figure 12). On line VI-84-01 (Figure 12a), between PKT 650 and 950, low-velocity zone between the *C* and *E* reflectors lies within inferred Wrangellia terrane rocks (Figure 12a). The cause for low velocities in forearc crustal rocks can be due to partial melt or the presence of fluids in the crust. Observed heat flow in this region is in agreement with the subduction thermal model [Hyndman and Wang, 1995] and the crustal temperature in this region is below 500°C. Hence the mapped low velocity is not due to melt in the lower crust and the most plausible explanation is the presence of fluids in the lower crust and upper mantle. Through seismic tomography study, Zhao *et al.* [2001] report a similar relative low-velocity region at this location and suggest that the *E* reflector (Figures 12a and 12b) may be due to the hydration of the forearc mantle and lower crust.

[40] The depth to the top of the Juan de Fuca crust, as interpreted from the tomographic velocity model and constrained by earthquake hypocenters, correlates well with the depth of the *F* reflector (Figures 12a and 12b) previously identified on the seismic reflection sections [Hyndman *et al.*, 1990; Tréhu *et al.*, 2002]. Calvert [2004] interpreted two megathrusts beneath Vancouver Island using seismic reflection data and correlated the *F* reflector to the top of the subducting Juan de Fuca crust. Nedimovi *et al.* [2003], however, interpreted the *F* reflector as the Moho of the subducting Juan de Fuca plate and argued for a shallower position of the Juan de Fuca crust beneath Vancouver Island. Nicholson *et al.* [2004] inverted teleseismic *P* wave coda to image fine-scale shear velocity structure and sug-

gested that the *E* reflector (above the *F* reflector) represents the subducted oceanic crust. Their interpretation places the top of the subducted oceanic crust at least 12 km shallower than previous interpretations that position the top of the oceanic crust to coincide with the *F* reflector. Our estimated depth of ~ 44 km to the top of the Juan de Fuca crust beneath earthquake recording station ALB (Figure 12a) is consistent with the estimate of 47 ± 3 km by Cassidy and Ellis [1991] from receiver function analysis and correlates the *F* reflector to the top of the oceanic crust.

[41] The forearc mantle wedge corner is identified on the velocity cross sections along the seismic reflection profiles, but no continental Moho reflections are observed on these lines. The gradual increase in velocity from lower crust to upper mantle on the overriding North American plate offers a possible explanation for the absence of seismic reflections and/or seismic refraction head waves from the continental Moho. Similarly, the contact between the top of the Juan de Fuca plate and the overlying forearc mantle along the subduction thrust is not clearly identified on the seismic reflection sections or on the tomographic velocity cross sections. This absence may be explained by the presence of a small vertical velocity gradient at this boundary between the serpentinized peridotites and eclogitized oceanic crust having similar velocities.

6. Summary

[42] The 3-D *P* wave velocity model constructed in this study from joint tomographic inversion of earthquake and active source travel times provides reliable definition of the forearc and the subduction zone velocity structure beneath southwestern British Columbia and adjoining inland waterways. Better relocation of future earthquakes in the region is possible with the new 3-D velocity model. The tomographic velocity model will provide enhanced constraints on modeling and characterizing the dehydration reactions in the slab crust and mantle, and provide new insights on the occurrence of large intraslab earthquakes in the northern Cascadia subduction zone.

[43] Higher than average velocities of 6.5–7.2 km/s observed in the mid to lower Wrangellian crust are attributed to the presence of mafic and possibly ultramafic rocks typically observed at other island arc terranes. Higher-velocity anomalies associated with the oceanic Crescent terrane are inferred to extend down to at least 20 km beneath southern Vancouver Island. Three mafic and/or ultramafic high-velocity bodies, with *P* wave velocity of 7.0–7.5 km/s, are observed beneath Barkley Sound, southern Vancouver Island and central Puget Sound at depths of approximately 25 km. They may represent gabbro members of the underthrust oceanic Crescent terrane. The Cascadia accretionary sedimentary prism underthrusts the Crescent terrane offshore Vancouver Island and to the south the Olympic Subduction Complex rocks are exposed on the Olympic Peninsula where the “Crescent backstop” bends landward in an arcuate trend. East of the Olympic peninsula, the Olympic Subduction Complex is thrust beneath the forearc crust to depths of ~ 40 km.

[44] A broad low-velocity zone of 7.2–7.5 km/s is imaged at depths of 37–45 km above the Juan de Fuca plate, similar to the low velocity zones observed in the

forearc mantle beneath central Japan, northern Costa Rica, eastern Aleutians, and the Andes. The low forearc mantle velocity in the Cascadia margin suggests widespread hydration, and upper mantle serpentinization of 15–20%. Earthquakes in the Juan de Fuca slab beneath Vancouver Island and adjoining waterways are reliably constrained by the 3-D velocity model. Velocity structure and relocated intraslab earthquakes are employed to define the position of the subduction thrust interface beneath Vancouver Island. Beneath southern Vancouver Island, the Juan de Fuca plate has dips of $\sim 11^\circ$, 16° , and 27° at depths of 30, 40, and 50 km, respectively. The change in dip of the Juan de Fuca plate beneath the Strait of Georgia from 16° to 27° at about 40–50 km depth corresponds well with expected depth of the basalt to eclogite phase change in the subducting Juan de Fuca crust that results in substantial densification of the crust.

[45] **Acknowledgments.** K.R. is thankful to Colin Zelt for helping with the programming details of First Arrival Seismic Tomography code and Taimi Mulder for providing the earthquake catalog. We thank Geoff Abers and two anonymous reviewers for their helpful reviews of this paper. An earlier version of the manuscript was improved by reviews from Patricia McCrory and Richard Blakely. This research was supported by a Natural Sciences and Engineering Research Council (NSERC) of Canada research grant and by the Earthquake and Coastal and Marine Programs of the U.S. Geological Survey. All figures were made using the Generic Mapping Tools [Wessel and Smith, 1991, 1995].

References

- Benz, H. M., B. A. Chouet, P. B. Dawson, J. C. Lahr, R. A. Page, and J. A. Hole (1997), Three-dimensional *P* and *S* wave velocity structure of Redoubt Volcano, Alaska, *J. Geophys. Res.*, *101*, 8111–8128.
- Bostock, M. G., R. D. Hyndman, S. Rondenay, and S. M. Peacock (2002), An inverted continental Moho and the serpentinization of the forearc mantle, *Nature*, *417*, 536–538.
- Brandon, M. T., and A. R. Calderwood (1990), High-pressure metamorphism and uplift of the Olympic subduction complex, *Geology*, *18*, 1252–1255.
- Brandon, M. T., and A. R. Calderwood (1998), Late Cenozoic exhumation of the Cascadia accretionary wedge in the Olympic Mountains, northwest Washington State, *Geol. Soc. Am. Bull.*, *110*, 985–1009.
- Brocher, T. M., and N. I. Christensen (2001), Density and velocity relationships for digital sonic and density logs from coastal Washington and laboratory measurements of Olympic peninsula mafic rocks and greynwacks, *U.S. Geol. Surv. Open File Rep.*, *01-264*.
- Brocher, T. M., et al. (1999), Wide-angle seismic recordings from the 1998 Seismic Hazards Investigation of Puget Sound (SHIPS), western Washington and British Columbia, *U.S. Geol. Surv. Open File Rep.*, *99-314*, 110 pp.
- Brocher, T. M., T. Parsons, R. A. Blakely, N. I. Christensen, M. A. Fisher, R. E. Wells, and the SHIPS Working Group (2001), Upper crustal structure in Puget Lowland, Washington: Results from 1998 Seismic Hazards Investigation of Puget Sound, *J. Geophys. Res.*, *106*, 13,541–13,564.
- Brocher, T. M., T. Parsons, A. M. Tréhu, C. M. Snelson, and M. A. Fisher (2003), Seismic evidence for widespread serpentinized forearc upper mantle along the Cascadia margin, *Geology*, *31*, 267–270.
- Calvert, A. J. (1996), Seismic reflection constraints on imbrication and underplating of the northern Cascadia convergent margin, *Can. J. Earth Sci.*, *33*, 1284–1307.
- Calvert, A. J. (2004), Seismic reflection imaging of two megathrust shear zones in the northern Cascadia subduction zone, *Nature*, *428*, 163–167.
- Cassidy, J. F. (1995), A comparison of the receiver structure beneath stations of the Canadian National Seismograph Network, *Can. J. Earth Sci.*, *32*, 938–951.
- Cassidy, J. F., and R. M. Ellis (1991), Shear wave constraints on a deep crustal reflective zone beneath Vancouver Island, *J. Geophys. Res.*, *96*, 19,843–19,851.
- Cassidy, J. F., and R. M. Ellis (1993), *S* wave velocity structure of the northern Cascadia subduction zone, *J. Geophys. Res.*, *98*, 4407–4421.
- Cassidy, J. F., G. C. Rogers, and F. Waldhauser (2000), Characterization of active faulting beneath the Strait of Georgia, British Columbia, *Bull. Seismol. Soc. Am.*, *90*, 1188–1199.

- Christensen, N. I., and W. D. Mooney (1995), Seismic velocity structure and composition of the continental crust: A global view, *J. Geophys. Res.*, *100*, 9761–9788.
- Clowes, R. M., M. T. Brandon, A. G. Green, C. J. Yorath, A. Sutherland-Brown, E. R. Kanasewich, and C. S. Spencer (1987), LITHOPROBE southern Vancouver Island: Cenozoic subduction complex imaged by deep seismic reflections, *Can. J. Earth Sci.*, *24*, 31–51.
- Clowes, R. M., D. J. Baird, and S. A. Dehler (1997), Crustal structure of the Cascadia subduction zone, southwestern British Columbia, from potential field and seismic studies, *Can. J. Earth Sci.*, *34*, 317–335.
- Dehler, S. A., and R. M. Clowes (1992), Integrated geophysical modelling of terranes and other structural features along the western Canadian margin, *Can. J. Earth Sci.*, *29*, 1492–1508.
- DeShon, H. R., and S. Y. Schwartz (2004), Evidence for serpentinization of the forearc mantle wedge along the Nicoya Peninsula, Costa Rica, *Geophys. Res. Lett.*, *31*, L21611, doi:10.1029/2004GL021179.
- Drew, J. J., and R. M. Clowes (1990), A re-interpretation of the seismic structure across the active subduction zone of western Canada, in *Studies of Laterally Heterogeneous Structures Using Seismic Refraction and Reflection Data, Proceedings of the 1987 Commission on Controlled Source Seismology Workshop*, edited by A. G. Green, *Pap. Geol. Surv. Can.*, *89-13*, 115–132.
- England, T. D. J., and R. M. Bustin (1998), Architecture of the Georgia Basin, southwestern British Columbia, *Bull. Can. Pet. Geol.*, *46*, 288–320.
- Fisher, M. A., et al. (1999), Seismic survey probes urban earthquake hazards in Pacific Northwest, *Eos Trans. AGU*, *80(2)*, 13, 16–17.
- Fliedner, M. M., and S. L. Klempner (1999), Structure of an island arc: Wide-angle seismic studies in the eastern Aleutian Islands, Alaska, *J. Geophys. Res.*, *104*, 10,667–10,694.
- Graeber, F. M., and G. Asch (1999), Three-dimensional models of P wave velocity and P-to-S velocity ratio in the southern central Andes by simultaneous inversion of local earthquake data, *J. Geophys. Res.*, *104*, 20,237–20,256.
- Graindorge, D., G. Spence, P. Charvis, J. Y. Collot, R. Hyndman, and A. M. Tréhu (2003), Crustal structure beneath the Strait of Juan de Fuca and southern Vancouver Island from seismic and gravity analyses, *J. Geophys. Res.*, *108(B10)*, 2484, doi:10.1029/2002JB001823.
- Hacker, B. R., S. M. Peacock, G. A. Abers, and S. D. Holloway (2003), Subduction factory: 2. Are intermediate-depth earthquakes in subducting slabs linked to metamorphic dehydration reactions?, *J. Geophys. Res.*, *108*, 2030, doi:10.1029/2001JB001129.
- Hole, J. A., and B. C. Zelt (1995), Three-dimensional finite difference reflection travel times, *Geophys. J. Int.*, *121*, 427–434.
- Hyndman, R. D. (1988), Dipping seismic reflectors, electrically conductive zones, and trapped water in the crust over a subducting plate, *J. Geophys. Res.*, *93*, 13,391–13,405.
- Hyndman, R. D., and S. M. Peacock (2003), Serpentinization of the forearc mantle, *Earth Planet. Sci. Lett.*, *212*, 417–432.
- Hyndman, R. D., and K. Wang (1995), The rupture zone of Cascadia great earthquakes from current deformation and the thermal regime, *J. Geophys. Res.*, *100*, 22,133–22,154.
- Hyndman, R. D., C. J. Yorath, R. M. Clowes, and E. E. Davis (1990), The northern Cascadia Subduction Zone at Vancouver Island: Seismic structure and tectonic history, *Can. J. Earth Sci.*, *27*, 313–329.
- Johnson, S. Y. (1984), Evidence for a margin truncating transcurrent fault (pre-late Eocene) in western Washington, *Geology*, *12*, 538–541.
- Jones, D. L., N. J. Silberling, and J. Hillhouse (1977), Wrangellia—A displaced terrane in northwestern North America, *Can. J. Earth Sci.*, *14*, 2565–2577.
- Kamiya, S., and Y. Kobayashi (2000), Seismological evidence for the existence of serpentinized wedge mantle, *Geophys. Res. Lett.*, *27*, 819–822.
- Kirby, S. H., E. R. Engdahl, and R. Denlinger (1996), Intraslab earthquakes and arc volcanism: Dual physical expressions of crustal and uppermost mantle metamorphism in subducting slabs, in *Subduction: Top to bottom*, *Geophys. Monogr. Ser.*, vol. 96, edited by G. E. Bebout et al., pp. 195–214, AGU, Washington, D. C.
- Kurtz, R. D., J. M. DeLaurier, and J. C. Gupta (1990), The electrical conductivity distribution beneath Vancouver Island: A region of active plate subduction, *J. Geophys. Res.*, *95*, 10,929–10,946.
- Massey, J. E. (1986), The Metchosin Igneous Complex, southern Vancouver Island: Ophiolite stratigraphy developed in an emergent setting, *Geology*, *14*, 602–605.
- McMechan, G. A., and G. D. Spence (1983), P-wave velocity structure of the Earth's crust beneath Vancouver Island, *Can. J. Earth Sci.*, *20*, 742–752.
- Miller, D. J., and N. I. Christensen (1994), Seismic signature and geochemistry of an island arc: A multidisciplinary study of the Kohistan accreted terrane, northern Pakistan, *J. Geophys. Res.*, *99*, 11,623–11,642.
- Miller, K. C., G. R. Keller, J. M. Gridley, J. H. Luetgert, W. D. Mooney, and H. Thybo (1997), Crustal structure along the west flank of the Cascades, western Washington, *J. Geophys. Res.*, *102*, 17,857–17,873.
- Monger, J. W. H. (1990), Georgia Basin—Regional setting and adjacent Coast Mountains geology, British Columbia, *Current Research, Part F, Pap. Geol. Surv. Can.*, *90-1F*, 95–108.
- Monger, J. W. H., R. A. Price, and D. J. Tempelman-Kluit (1982), Tectonic accretion and the origin of the two major metamorphic and plutonic belts in the Canadian Cordillera, *Geology*, *10*, 70–75.
- Mooney, W. D., and R. Meissner (1991), Continental crustal evolution observations, *Eos Trans. AGU*, *72(48)*, 537, 540–541.
- Mosher, D. C., J. F. Cassidy, C. Lowe, Y. Mi, R. D. Hyndman, G. C. Rogers, and M. A. Fisher (2000), Neotectonics in the Strait of Georgia: Tentative correlation of seismicity with shallow geologic structure in southwestern British Columbia, Geological Survey of Canada, *Current Research, 2000-A22*, pp. 1–9, Geol. Surv. of Can., Ottawa, Ont.
- Muller, J. E. (1977), Evolution of the Pacific Margin, Vancouver Island, and adjacent regions, *Can. J. Earth Sci.*, *14*, 2062–2085.
- Muller, J. E. (1980), Chemistry and Origin of Eocene Metchosin Volcanics, Vancouver Island, British Columbia, *Can. J. Earth Sci.*, *17*, 199–209.
- Myers, S. C., S. Beck, G. Zandt, and T. Wallace (1998), Lithospheric-scale structure across the Bolivian Andes from tomographic images of velocity and attenuation for P and S waves, *J. Geophys. Res.*, *103*, 21,233–21,252.
- Nedimović, M. R., R. D. Hyndman, K. Ramachandran, and G. D. Spence (2003), Reflection signature of seismic and aseismic slip on the northern Cascadia subduction interface, *Nature*, *424*, 416–420.
- Nicholson, T. A., M. G. Bostock, and J. F. Cassidy (2004), Structure of the Northern Cascadia Subduction Zone, *Eos Trans. AGU*, *85(17)*, Joint Assembly Suppl., Abstract S23B-05.
- Parsons, T., A. M. Tréhu, J. H. Luetgert, K. Miller, F. Kilbride, R. E. Wells, M. A. Fisher, E. Flueh, U. S. ten Brink, and N. I. Christensen (1998), A new view into the Cascadia subduction zone and volcanic arc: Implications for earthquake hazards along the Washington margin, *Geology*, *26*, 199–202.
- Parsons, T., R. E. Wells, E. Flueh, U. S. ten Brink, and M. A. Fisher (1999), Three-dimensional velocity structure of Siletzia and other accreted terranes in the Cascadia fore arc of Washington, *J. Geophys. Res.*, *104*, 18,015–18,039.
- Peacock, S. M. (2001), Are double seismic zones caused by serpentine dehydration reactions in subducting oceanic mantle?, *Geology*, *29*, 299–302.
- Peacock, S. M., and R. D. Hyndman (1999), Hydrous minerals in the mantle wedge and the maximum depth of subduction thrust earthquakes, *Geophys. Res. Lett.*, *26*, 2517–2520.
- Peacock, S. M., K. Wang, and A. M. McMahon (2002), Thermal structure and metamorphism of subducting oceanic crust: Insight into Cascadia intraslab earthquakes, in *The Cascadia Subduction Zone and Related Subduction Systems—Seismic Structure, Intraslab Earthquakes and Processes, and Earthquake Hazards*, edited by S. Kirby, K. Wang, and S. Dunlop, Open File 4350, pp. 123–126, Geol. Surv. of Can., Ottawa, Ont.
- Ramachandran, K. (2001), Velocity structure of S.W. British Columbia and N.W. Washington from 3-D non-linear seismic tomography, Ph.D. thesis, Univ. of Victoria, Victoria, B. C., Canada.
- Ramachandran, K., S. E. Dosso, C. A. Zelt, G. D. Spence, R. D. Hyndman, and T. M. Brocher (2004), Upper crustal structure of southwestern British Columbia from the 1998 Seismic Hazards Investigation in Puget Sound, *J. Geophys. Res.*, *109*, B09303, doi:10.1029/2003JB002826.
- Riddiough, R. P. (1979), Gravity and structure of an active margin—British Columbia and Washington, *Can. J. Earth Sci.*, *14*, 384–396.
- Riddiough, R. P., and R. D. Hyndman (1991), Modern plate tectonic regime of the continental margin of western Canada, in *Geology of North America*, vol. G-2, *Geology of the Cordilleran Orogen in Canada*, edited by H. Gabrielse and C. J. Yorath, Geology of Canada, *4*, 435–455, Geol. Surv. of Can., Ottawa, Ont.
- Rogers, G. C. (1983), Seismotectonics of British Columbia, Ph.D. thesis, Univ. of B. C., Vancouver, Canada.
- Rogers, G. C. (1998), Earthquakes and earthquake hazard in the Vancouver area, in *Geology and Natural Hazards of the Fraser River Delta, British Columbia*, edited by J. J. Clague, J. L. Luternauer, and D. C. Mosher, *Geol. Surv. Can. Bull.*, *525*, 17–25.
- Rogers, G. C., and H. S. Hasegawa (1978), A second look at the British Columbia earthquake of 23 June, 1946, *Bull. Seismol. Soc. Am.*, *68*, 653–676.
- Shaw, P. R., and J. A. Orcutt (1985), Waveform inversion of seismic refraction data and applications to young Pacific crust, *Geophys. J. R. Astron. Soc.*, *82*, 375–414.

- Smith, P. L., and H. W. Tipper (1986), Plate tectonics and palaeobiogeography: Early Jurassic (Pliensbachian) endemism and diversity, *Palaios*, *1*, 399–412.
- Spence, G. D., R. M. Clowes, and R. M. Ellis (1985), Seismic structure across the active subduction zone of western Canada, *J. Geophys. Res.*, *90*, 6754–6772.
- Stanley, D., A. Villasenor, and H. Benz (1999), Subduction zone and crustal dynamics of western Washington: A tectonic model for earthquake hazards evaluation, *U.S. Geol. Surv. Open File Rep.* 99-311.
- Symons, N. P., and R. S. Crosson (1997), Seismic velocity structure of the Puget Sound region from 3-D non-linear tomography, *Geophys. Res. Lett.*, *24*, 2593–2596.
- Toomey, D. R., S. C. Solomon, and G. M. Purdy (1994), Tomographic imaging of the shallow crustal structure of the East Pacific Rise at 9°30'N, *J. Geophys. Res.*, *99*, 24,135–24,157.
- Tréhu, A. M., I. Asudeh, T. M. Brocher, J. H. Luetgert, W. D. Mooney, J. L. Nabelek, and Y. Nakamura (1994), Crustal architecture of the Cascadia forearc, *Science*, *266*, 237–243.
- Tréhu, A. M., T. M. Brocher, K. C. Creager, M. A. Fisher, L. Preston, and G. D. Spence (2002), Geometry of the subducting Juan de Fuca Plate: New constraints from SHIPS98, in *The Cascadia Subduction Zone and Related Subduction Systems: Seismic Structure, Intraslab Earthquakes and Processes, and Earthquake Hazards*, edited by S. Kirby, K. Wang, and S. Dunlop, *Open File 4350*, pp. 25–32, Geol. Surv. of Can., Ottawa, Ont.
- Van Wagoner, T. M., R. S. Crosson, K. C. Creager, G. Medema, L. Preston, N. P. Symons, and T. M. Brocher (2002), Crustal structure and relocated earthquakes in the Puget Lowland, Washington, from high-resolution seismic tomography, *J. Geophys. Res.*, *107*(B12), 2381, doi:10.1029/2001JB000710.
- Vidale, J. E. (1990), Finite-difference calculation of traveltimes in three dimensions, *Geophysics*, *55*, 521–526.
- Wessel, P., and W. H. F. Smith (1991), Free software helps map and display data, *Eos Trans. AGU*, *72*, 445–446.
- Wessel, P., and W. H. F. Smith (1995), New version of the Generic Mapping Tools released, *Eos Trans. AGU*, *76*, 329.
- White, W. R. H., and J. C. Savage (1965), A seismic refraction and gravity study of the earth's crust in British Columbia, *Bull. Seismol. Soc. Am.*, *55*, 463–486.
- Yorath, C. J., and H. W. Nasmith (1995), *Geology of Southern Vancouver Island*, Orca, Victoria, Canada.
- Zelt, B. C., R. M. Ellis, C. A. Zelt, R. D. Hyndman, C. Lowe, G. D. Spence, and M. A. Fisher (2001), Three dimensional crustal velocity structure beneath the Strait of Georgia, British Columbia, *Geophys. J. Int.*, *144*, 695–712.
- Zelt, C. A., and P. J. Barton (1998), Three-dimensional seismic refraction tomography: A comparison of two methods applied to data from the Faeroe Basin, *J. Geophys. Res.*, *103*, 7187–7210.
- Zhao, D. (2001), Seismological structure of subduction zones and its implications for arc magmatism and dynamics, *Phys. Earth Planet. Inter.*, *127*, 197–214.
- Zhao, D., K. Wang, G. C. Rogers, and S. M. Peacock (2001), Tomographic image of low P velocity anomalies above slab in northern Cascadia subduction zone, *Earth Planets Space*, *53*, 285–293.

T. M. Brocher, U.S. Geological Survey, MS 977, 345 Middlefield Road, Menlo Park, CA 94025, USA. (brocher@usgs.gov)

S. E. Dosso and G. D. Spence, School of Earth and Ocean Sciences, University of Victoria, Victoria, BC, Canada V8W 3P6. (sdosso@uvic.ca; gspence@uvic.ca)

R. D. Hyndman and K. Ramachandran, Pacific Geoscience Centre, Geological Survey of Canada, 9860 W Saanich Road, Sidney, BC, Canada V8L 4B2. (hyndman@pgc.nrcan.gc.ca; kramacha@nrcan.gc.ca)